Structure of solid-state systems from embedded-cluster calculations: A divide-and-conquer approach

Tianhai Zhu
Department of Chemistry, Duke University, Durham, North Carolina 27708

Wei Pan
Department of Chemistry, Duke University, Durham, North Carolina 27708;
Institute of Solid State Physics, Chinese Academy of Sciences, Hefei 230031, China;
and International Center for Materials Physics, Chinese Academy of Sciences, Shenyang 110015, China

Weitao Yang
Department of Chemistry, Duke University, Durham, North Carolina 27708
(Received 14 June 1995; revised manuscript received 22 December 1995)

The first-principles divide-and-conquer density-functional approach has been extended to solid-state systems. The method has the following features. (1) It divides a periodic solid-state system into equivalent primitive cells and further divides each cell into subsystems. The electron density of each subsystem is determined through the local representation of the one-electron Hamiltonian and used to form the total density per primitive cell. The method calculates the electronic structure of solids without involving the reciprocal space and its associated band structure. (2) It uses numerical atomic orbitals as basis functions with great variational flexibility. The Hamiltonian and other matrix elements are evaluated by numerical integration without any shape approximation to the effective one-electron potential. (3) This method, based on real space partition, can be applied to extended solid-state systems without translational symmetry, such as defects and surface chemisorption. As the first step, we have applied and tested the method to the electronic structure calculations of various crystalline solids: metallic lithium and copper, ionic sodium chloride, and covalent diamond and silicon. The self-consistently computed cohesive energies, structural properties, and density of states are in good agreement with those from the local-density approximation band-structure calculations and experimental results.

I. INTRODUCTION

The past two decades have seen tremendous progress in the development of first-principles band-structure calculations based on Kohn-Sham density-functional theory[1–4] (DFT) for periodic solid-state systems.[5–22] To date, a variety of such computational techniques have emerged to make it possible to accurately predict ground-state properties of simple solids. Despite the great success of modern first-principles band-structure calculations on solids, the computational effort normally scales as the cube of the number of atoms per unit cell and consequently limits the size of system which can be studied.

For extended solid-state systems without translational symmetry, such as defects in crystals, reconstructed solid surfaces, adsorption, and chemical reactions on surfaces, band-structure methods are usually not very efficient. There are many other theoretical approaches for these extended systems.[23–33] In particular, various embedded-cluster approaches are widely used.[28–33] The basic assumption in this kind of approach is that the electronic structure of an extended system can be established as the result of local interactions. These methods have proved to be very useful in the studies of defects in crystals, adsorption, and chemical reactions on surfaces. A major problem in the embedding scheme is how to take the boundary effects into consideration rigorously. The computational effort in all these methods for extended systems again scales as the cube of the number of atoms involved in the region of interest. This rapid scaling is the ultimate bottleneck for the applications of these methods to large systems.

To break the N^3-scaling bottleneck, we have recently developed the linear scaling divide-and-conquer method[34] for large molecules: divide a large molecule into subsystems, determine the electron density of each subsystem separately, and sum the corresponding contributions from subsystems to obtain the total density and energy. We have demonstrated in many tests that with the increasing use of buffer atoms (neighboring atoms for each subsystem) the divide-and-conquer method can reproduce the corresponding Kohn-Sham results.[35–37] A great deal of effort has been subsequently devoted to the search for order-N algorithms for large scale electronic structure calculations.[38–51] We expect these linear scaling methods to significantly enhance our ability to perform *ab initio* calculations on large systems.

Since the computational effort in the divide-and-conquer approach scales linearly with the system size, it has the potential for application to complex solid-state systems. In this paper we particularly focus on the implementation of the method for periodic solid-state systems. In principle, such an implementation should enable us to calculate the electronic structure of periodic crystalline solids with large and complex unit cells without involving their band structures. We want to point out here that the current implementation of the

divide-and-conquer method is an all-electron one. We also expect the divide-and-conquer method to become a rigorous and efficient approach for *ab initio* calculations of extended systems where the translational symmetry is broken. We can divide an extended system into subsystems and calculate explicitly the electron densities for those subsystems in the physical region of interest. In this sense the divide-and-conquer method is similar to the embedding schemes.[28–33] We want to emphasize here that in this ''divide-and-conquer embedding,'' the boundary effects can be taken into consideration in a systematic fashion by including the contributions of more and more neighboring atoms. The charge transfer between the region of interest and the environment is effected by the chemical potential equalization.

The remainder of this article is organized as follows. In Sec. II we briefly review the recent development of the divide-and-conquer method. We then present the implementation of this approach for solid-state computations in Sec. III. In Sec. IV we compare our results for metallic lithium and copper, ionic sodium chloride, and covalent diamond and silicon with those from the local-density approximation (LDA) band-structure calculations and experimental values. We provide some concluding remarks in Sec. V.

II. THE DIVIDE-AND-CONQUER METHOD

Most of the contemporary electronic structure calculations for solid-state systems are based on the Hohenberg-Kohn-Sham density-functional theory. In the Kohn-Sham method,[52] the ground-state electron density of an N-electron system is expressed as

$$\rho(\vec{r})=2\sum_{i=1}^{N/2}|\psi_i(\vec{r})|^2, \tag{1}$$

where $\psi_i(\vec{r})$ is the Kohn-Sham orbital satisfying the equation

$$\hat{H}\psi_i(\vec{r})=[-\tfrac{1}{2}\nabla^2+v_{\rm eff}(\vec{r})]\psi_i(\vec{r})=\varepsilon_i\psi_i(\vec{r}), \tag{2}$$

with $v_{\rm eff}(\vec{r})$ as the effective one-electron potential. The total energy is given by

$$E[\rho]=2\sum_{i=1}^{N/2}\varepsilon_i+Q[\rho]+\sum_{A>B}\frac{Z_AZ_B}{R_{AB}}, \tag{3}$$

where

$$Q[\rho]=\int\rho(\vec{r})[-\tfrac{1}{2}\phi(\vec{r})-v_{\rm xc}(\vec{r})]d\vec{r}+E_{\rm xc}[\rho], \tag{4}$$

$\phi(\vec{r})=\int\rho(\vec{r}')/|\vec{r}-\vec{r}'|d\vec{r}'$ is the Coulomb potential, and $v_{\rm xc}(\vec{r})=\delta E_{\rm xc}[\rho]/\delta\rho$ is the exchange-correlation potential. With the local-density approximation (LDA),[3]

$$E_{\rm xc}[\rho]=\int\rho(\vec{r})\varepsilon_{\rm xc}(\vec{r})d\vec{r}, \tag{5}$$

where $\varepsilon_{\rm xc}(\vec{r})$ is the exchange-correlation energy density. Equations (1) and (2) have to be solved self-consistently to find the ground-state energy and electron density.

The global orbital representation of the electron density in the Kohn-Sham approach causes the computational effort to scale as N^3. But the electron density is a local variable. To accurately represent the density locally, we do not need the delocalized Kohn-Sham orbitals. Much simplification can be achieved via a divide-and-conquer approach without losing the Kohn-Sham accuracy.[34] The method is based on a well-known expression for the electron density,[3]

$$\rho(\vec{r})=2\langle\vec{r}|\,\eta(\mu-\hat{H})|\vec{r}\rangle, \tag{6}$$

where $\eta(x)$ is the Heaviside step function and μ is the chemical potential, which is related to the density normalization. We divide a system into subsystems by the following smooth partition:

$$1=\sum_\alpha p^\alpha(\vec{r}),$$

where $p^\alpha(\vec{r})$ is a positive weighting function for the subsystem α. The total density now reads

$$\rho(\vec{r})=2\sum_\alpha p^\alpha(\vec{r})\langle\vec{r}|\,\eta(\mu-\hat{H})|\vec{r}\rangle=\sum_\alpha\rho^\alpha(\vec{r}), \tag{7}$$

where the subsystem density is defined as

$$\rho^\alpha(\vec{r})=2p^\alpha(\vec{r})\langle\vec{r}|\,\eta(\mu-\hat{H})|\vec{r}\rangle. \tag{8}$$

We now make the local approximation to the Kohn-Sham Hamiltonian in Eq. (8):

$$\tilde{\rho}^\alpha(\vec{r})=2p^\alpha(\vec{r})\langle\vec{r}|f_\beta(\mu-\hat{H}^\alpha)|\vec{r}\rangle, \tag{9}$$

where $f_\beta(x)$ is the Fermi function $\{f_\beta(x)=[1+\exp(-\beta x)]^{-1}\}$ and $\hat{H}^\alpha$ is the subspace approximation of $\hat{H}$. We then represent $\hat{H}^\alpha$ as well as the subsystem eigenfunctions $\{\psi_i^\alpha\}$ in terms of the nonorthogonal basis functions $\{\phi_j^\alpha\}$ that are localized in the subsystem α:

$$\hat{H}^\alpha=\sum_i|\psi_i^\alpha\rangle\varepsilon_i^\alpha\langle\psi_i^\alpha|, \tag{10}$$

$$\psi_i^\alpha(\vec{r})=\sum_j C_{ji}^\alpha\phi_j^\alpha(\vec{r}), \tag{11}$$

where $\{\varepsilon_i^\alpha\}$ and $\{\psi_i^\alpha\}$ are found by solving the matrix equation

$$(\underline{\underline{H}}^\alpha-\varepsilon_i^\alpha\underline{\underline{S}}^\alpha)\underline{C}_i^\alpha=0, \tag{12}$$

with the matrix elements given by

$$H_{ij}^\alpha=\langle\phi_i^\alpha|\hat{H}|\phi_j^\alpha\rangle,\quad S_{ij}^\alpha=\langle\phi_i^\alpha|\phi_j^\alpha\rangle. \tag{13}$$

The expression of the total electron density now becomes

$$\tilde{\rho}(\vec{r})=\sum_\alpha\tilde{\rho}^\alpha(\vec{r})=2\sum_\alpha p^\alpha(\vec{r})\sum_i f_\beta(\mu-\varepsilon_i^\alpha)|\psi_i^\alpha(\vec{r})|^2, \tag{14}$$

with μ determined by the normalization constraint

$$N=\int\tilde{\rho}(\vec{r})d\vec{r}=2\sum_\alpha\sum_i f_\beta(\mu-\varepsilon_i^\alpha)\langle\psi_i^\alpha|p^\alpha(\vec{r})|\psi_i^\alpha\rangle. \tag{15}$$

TABLE I. The buffer schemes for lithium, copper, diamond, silicon, and sodium chloride calculations. For each element, the first column gives the number of buffer atoms for each buffer scheme and the second column indicates the distance (a.u.) between the buffer atoms and the subsystem.

Buffer schemes	Li		Cu		Diamond		Si		NaCl	
1	8	5.713	12	4.811	4	2.913	4	4.443	6	5.320
2	26	9.329	18	6.803	16	4.757	16	7.256	18	7.523
3	58	11.426	42	8.332	34	6.727	34	10.261	26	9.214
4	88	14.377	54	9.621	46	7.331	46	11.181	32	10.639
5	112	14.751	78	10.757	70	8.239	70	12.567	56	11.895
6			86	11.783	86	8.739	86	13.329	80	13.030

The eigenvalue summation in Eq. (3) is replaced by

$$\tilde{\varepsilon}=2\int \langle\vec{r}|\hat{H}\eta(\mu-\hat{H})|\vec{r}\rangle d\vec{r}$$

$$=\sum_{\alpha}\tilde{\varepsilon}^{\alpha}=2\sum_{\alpha}\sum_{i} f_{\beta}(\mu-\varepsilon_i^{\alpha})\varepsilon_i^{\alpha}\langle\psi_i^{\alpha}|p^{\alpha}|\psi_i^{\alpha}\rangle, \quad (16)$$

and the approximated total energy is

$$\tilde{E}=\tilde{\varepsilon}+Q[\tilde{\rho}]+\sum_{A>B}\frac{Z_A Z_B}{R_{AB}}. \quad (17)$$

Other electronic properties can also be calculated in the same manner. A quantity of interest is the density of electronic states (DOS), which has the following form in the divide-and-conquer method[35]

$$g(\varepsilon)=\frac{dN(\varepsilon)}{d\varepsilon}=2\sum_{\alpha}\sum_{i}\langle\psi_i^{\alpha}|p^{\alpha}|\psi_i^{\alpha}\rangle f'_{\beta}(\varepsilon-\varepsilon_i^{\alpha}), \quad (18)$$

where $f'_{\beta}(x)$ is the derivative of the Fermi function.

The subsystem density can be accurately represented with some local basis sets. The local basis set for a subsystem includes the atomic orbitals of the subsystem and its neighboring atoms which are called buffer atoms. The use of local basis sets is a truncation approximation, and the buffer atoms provide a systematic way to reduce the error associated with the truncation. The N^3-scaling computational bottleneck in the Kohn-Sham (KS) scheme has thus been eliminated because the divide-and-conquer method does not employ the global Kohn-Sham orbital representation of the total electron density. Various molecular test calculations have shown that in general the divide-and-conquer method with proper buffer atom schemes is capable of reproducing the corresponding Kohn-Sham results.[35–37]

III. EXTENSION TO SOLID-STATE SYSTEMS

Since the divide-and-conquer method is a general approach for large systems, as the first step, we here extend it to periodic crystalline solids. We will follow the general procedures outlined by Yang and Zhou for the extension of the method to periodic solids.[53] The most important characteristic of the crystalline solids is the periodicity. The whole system can be constructed from a representative cell — the primitive cell.

A. Division and buffer schemes

To take advantage of the periodicity we divide a solid into equivalent primitive cells and then further divide all primitive cells into subsystems in the same way. In principle, the partition of a primitive cell is arbitrary. For simplicity, in our current implementation we typically let the subsystem consist of a single atom. With this division we only need to calculate the densities of those subsystems within one primitive cell. The summations over the subsystems in Eqs. (14), (16), and (18) now become summations over primitive cells. In general, we have two summations: one over all primitive cells and the other over the subsystems in a primitive cell. Since solids are infinite systems, the quantities to be calculated are the total energy and density per primitive cell. We only need to perform summations over subsystems in one primitive cell in Eqs. (14), (16), and (18). In addition, the number of electrons in a primitive cell should be used in Eq. (15) to determine the proper normalization.

We define the general normalized partition function for subsystem α as the sum of the atomic partition functions over the atoms in subsystem α:

$$p^{\alpha}(\vec{r})=\sum_{A\in\alpha}p^{A}(\vec{r}), \quad (19)$$

where

$$p^{A}(\vec{r})=\frac{\rho_0^A(|\vec{r}-\vec{R}_A|)(e^{r_0/|\vec{r}-\vec{R}_A|}-1-r_0/|\vec{r}-\vec{R}_A|)}{\Sigma_B\rho_0^B(|\vec{r}-\vec{R}_B|)(e^{r_0/|\vec{r}-\vec{R}_B|}-1-r_0/|\vec{r}-\vec{R}_B|)} \quad (20)$$

with $r_0 = 0.5$ and $\rho_0^A(|\vec{r}-\vec{R}_A|)$ being the spherical atomic density for atom A located at $\vec{R}_A$. The summation in Eq. (20) is over all atoms in a solid. Other forms of partition functions can also be chosen. With this set of partition functions the total density can be decomposed into the contributions from subsystems in primitive cells.

For each subsystem in a primitive cell, its neighboring atoms are chosen as buffer atoms to form a set of buffer schemes according to their distances from the subsystem. We present in Table I the buffer schemes used in our calculations for lithium, copper, diamond, silicon, and sodium chloride. Note that some of the buffer atoms with different distances from a subsystem are grouped together so that there is a significant increase in the number of buffer atoms for adjacent buffer schemes.

B. Construction of the one-electron potential

In solids the crystal potential contains contributions from an infinite system. Many calculations have demonstrated that the LDA can provide an adequate treatment for the exchange-correlation effects in ground-state solids. Since the exchange-correlation potential depends on the density in a local way, direct summation can be carried out. We here focus on the construction of the electrostatic potential. To achieve convergent results, we need to calculate the nuclear and the electronic potential together. The long-range contribution to the electrostatic potential is generated by the deformation density $\rho_{\rm def}(\vec{r})$ defined as

$$\rho(\vec{r})=\rho_{\rm atomic}(\vec{r})+\rho_{\rm def}(\vec{r}), \tag{21}$$

where $\rho_{\rm atomic}(\vec{r})$ is the superposition of the atomic densities. The nuclear potential is

$$v_n(\vec{r})=-\sum_{\alpha}\sum_{A\in\alpha}\frac{Z_A}{|\vec{r}-\vec{R}_A|}, \tag{22}$$

and the total electrostatic potential is

$$v_n(\vec{r})+\phi(\vec{r})=\sum_{\alpha}\sum_{A\in\alpha}\left\{-\frac{Z_A}{|\vec{r}-\vec{R}_A|}+\int\frac{\rho_0^A(|\vec{r}'-\vec{R}_A|)}{|\vec{r}-\vec{r}'|}d\vec{r}'\right\}+\int\frac{\rho_{\rm def}(\vec{r}')}{|\vec{r}-\vec{r}'|}d\vec{r}', \tag{23}$$

where α is the cell index and A is the nuclear index. In Eq. (23) the summations are performed over the electrostatic potentials of neutral atoms, and are therefore short ranged and fast converging. The deformation density $\rho_{\rm def}(\vec{r})$ is represented on a real space multicenter numerical grid and cannot be integrated directly to get its potential. To compute the potential generated by the deformation density, we need to decompose the deformation density approximately into atomic contributions, and perform a multipolar expansion for each of them:[9]

$$\tilde{\rho}_{\rm def}(\vec{r})=\sum_A\rho_A^{\rm def}(\vec{r}-\vec{R}_A)=\sum_A\sum_{lm}\rho_{Alm}^{\rm def}(|\vec{r}-\vec{R}_A|)Y_l^m(\vec{r}-\vec{R}_A), \tag{24}$$

where $\rho_{Alm}^{\rm def}(|\vec{r}-\vec{R}_A|)$ is given by the projection

$$\rho_{Alm}^{\rm def}(s)=\int_{s=|\vec{r}-\vec{R}_A|}Y_l^m(\vec{r}-\vec{R}_A)p^A(\vec{r})\tilde{\rho}_{\rm def}(\vec{r})d\Omega. \tag{25}$$

Here the atomic partition function is defined in Eq. (20). With this choice of $p^A(\vec{r})$, the quantity $p^A(\vec{r})\tilde{\rho}_{\rm def}(\vec{r})$ is the atomic contribution to the deformation density. Following Eq. (14) for the determination of subsystem density $\tilde{\rho}^{\alpha}(\vec{r})$, $p^A(\vec{r})\tilde{\rho}_{\rm def}(\vec{r})$ is determined (on the integration grid) directly from the eigenvalues and eigenfunctions $\{\varepsilon_i^{\alpha},\psi_i^{\alpha}\}$ of the subsystem α to which atom A belongs. In this way we do not need to calculate the total density (by summing the subsystem contributions) and then partition the result to get the $p^A(\vec{r})\tilde{\rho}_{\rm def}(\vec{r})$. This procedure significantly saves CPU time. We also only need to calculate $p^A(\vec{r})\tilde{\rho}_{\rm def}(\vec{r})$ for those atoms in the representative primitive cell because of the periodicity. For the density at a given point in the central cell, the infinite summation in Eq. (24) can be terminated in a short-range space due to its fast convergence. From the expansion in Eq. (24) the deformation potential can be determined as

$$\int\frac{\tilde{\rho}_{\rm def}(\vec{r}')}{|\vec{r}-\vec{r}'|}d\vec{r}'=\sum_{\alpha}\sum_{A\in\alpha}\{v_A^{\rm short}(\vec{r}-\vec{R}_A)+v_A^{\rm long}(\vec{r}-\vec{R}_A)\}, \tag{26}$$

where

$$v_A^{\rm short}(\vec{r})=4\pi\sum_{lm}\frac{1}{2l+1}Y_l^m(\Omega_{\vec{r}})\left\{r^l\int_r^{\infty}\rho_{Alm}^{\rm def}(s)s^{1-l}ds-r^{-l-1}\int_r^{\infty}\rho_{Alm}^{\rm def}(s)s^{l+2}ds\right\}, \tag{27}$$

and

$$v_A^{\rm long}(\vec{r})=4\pi\sum_{lm}\frac{1}{2l+1}Y_l^m(\Omega_{\vec{r}})\times r^{-l-1}\int_0^{\infty}\rho_{Alm}^{\rm def}(s)s^{l+2}ds=4\pi\sum_{lm}\frac{Y_l^m(\Omega_{\vec{r}})}{2l+1}\frac{Q_{Alm}}{r^{l+1}}, \tag{28}$$

where Q_{Alm} is the multipole associated with atom A. The summation of the $v_A^{\rm short}$ term in Eq. (26) converges very fast and can be done in the short-range space (within the radius of $R_{\rm short}$ from the origin) as the deformation density. The summation of the $v_A^{\rm long}$ term contains the well-known Madelung sum. With the charge neutrality constraint in one primitive cell, the long-range summation is conditionally convergent for $l=0$. There exist many methods to deal with the conditional convergence problem for the Madelung sum (for example, see Ref. 10). In our calculations we have adopted the conventional Ewald technique[54] for the summation of the terms for $l=0$. To assess the accuracy of only including $l=0$ terms in the Madelung sum, we performed the long-range sum for all the terms with l up to 2, using the screening function method developed by te Velde and Baerends.[10] In this method, all the multipole lattice sums in Eq. (28) are evaluated in real space up to a cutoff radius, by weighting the contributions with a Fermi-like screening function depending on its distance to the central cell. Our test calculations for NaCl show that neglecting $l>0$ terms in the Madelung sum gives less than 10^{-4} hartree in error for the cohesive energy per primitive cell. It appears that for high-symmetry bulk structures the inclusion of $l>0$ terms in the Madelung sum is unlikely to have much effect on the calculations of cohesive properties. Therefore we have neglected those $l>0$ terms in all the test calculations presented in this paper. However, there are cases where the inclusion of $l>0$ terms would be important, e.g., calculations of the polarization in an external field, and our program is capable of including these terms where they are needed.

C. Integration and matrix evaluation

Our program uses the numerical Kohn-Sham atomic orbitals as basis functions.[36] All the multicenter integrals including those required for the construction of the Hamiltonian and other matrices are evaluated by Delley's three-dimensional multicenter numerical integration method.[9] The partition function defined in Eq. (20) is also employed in the numerical integration.[9] We need to pay special attention to the evaluation of the potential matrix elements since there is an infinite number of atoms in solids. This means we at least have to perform numerical integration to compute the nuclear potential matrix elements in the region where all basis functions have non-negligible values. Such a region in solids usually involves hundreds of atoms thus making the numerical integration extremely time consuming. To calculate the potential matrix more efficiently, we have adopted a very simple approach in the spirit of the local-projection method.[55] Define the following local-projection function:

$$\overline{p^{\alpha}}(\vec{r})=\prod_{A\notin\alpha}\{1-\exp(-k_A|\vec{r}-\vec{R}_A|^2)\} \tag{29}$$

where α is the subsystem index, A runs over all the atoms in the solid except for those atoms in subsystem α and the buffer atoms for subsystem α, $\vec{R}_A$ is the nuclear position of atom A in the solid, and k_A is a constant depending on the type of atoms and basis functions. The function serves to project away the singularities contributed from atoms other than the buffer atoms of subsystem α. The potential matrix for subsystem α is now computed in the following form:

$$V_{ij}^{\alpha}=\langle\phi_i^{\alpha}\overline{p^{\alpha}}\,|V|\,\phi_j^{\alpha}\rangle. \tag{30}$$

Outside the buffer region, $\overline{p^{\alpha}}(\vec{r})$ takes zero values at the singularities of the potential (the positions of atoms) and the integrand in Eq. (30) becomes smooth. Thus its numerical integration is performed with only those points generated from atoms within the buffer area of subsystem α.

The current approach smoothly removes the Coulomb potential singularities outside the buffer area for each subsystem. We do not expect this approach to have much impact on the accurate evaluation of the potential matrix, since the local-projection function defined in Eq. (29) is effective only within a very local region around each nucleus outside the buffer atoms. Test calculations in Sec. IV attest to this point. Viewed from a different angle, the approach can be considered as a modified local-projection method which uses different left-side and right-side basis sets.[55] If one of the basis sets is highly localized, the multicenter integrals can be reduced to single-center integrals. Several single-center projection functions have been proposed to obtain the localized basis set in the local-projection method.[55] In the current approach as shown in Eqs. (29) and (30), the integration is, instead, carried out with points generated from atoms within the buffer region of each subsystem.

D. Self-consistency and total energy

The self-consistent procedure in our solid-state calculations is as follows. (i) Divide a solid into primitive cells and subsystems in each cell; (ii) choose the partition function and atomic orbitals from the subsystem and surrounding buffer atoms to form a local basis set $\{\phi_i^{\alpha}\}$ for each subsystem α; (iii) superimpose the atomic densities as the initial total density to generate the effective one-electron potential; (iv) for each subsystem α, solve Eq. (12) to obtain $\{\varepsilon_i^{\alpha},\psi_i^{\alpha}\}$; (v) determine μ and $\rho(\vec{r})$ to obtain the new effective potential and repeat steps (iv) and (v) until self-consistency; (vi) finally, compute the total energy per unit cell. We need to modify Eq. (17) to compute the total energy per primitive cell. Since all the primitive cells are equivalent, we only need to sum over all subsystem contributions in one primitive cell (the central cell). The calculation of $\tilde{\varepsilon}$ per cell in Eq. (16) is straightforward. The second term $Q[\rho]$ and the nuclear repulsion term in Eq. (17) have to be combined together to give the convergent result. Rewrite the two terms as follows:

$$R=Q[\rho]+\sum_{A>B}\frac{Z_AZ_B}{R_{AB}}=R_1+R_2, \tag{31}$$

where

$$R_1=\int\rho(\vec{r})\left\{-\frac{1}{2}[\phi(\vec{r})+v_n(\vec{r})]-v_{\rm xc}(\vec{r})+\varepsilon_{\rm xc}(\vec{r})\right\}d\vec{r}, \tag{32}$$

and

$$R_2=\frac{1}{2}\int\rho(\vec{r})v_n(\vec{r})d\vec{r}+\sum_{A>B}\frac{Z_AZ_B}{R_{AB}}. \tag{33}$$

With the partition function $p^{\alpha}(\vec{r})$, we can easily find the per-primitive-cell quantities, R_1^{α} and R_2^{α},

$$R_1^{\alpha}=\int\rho(\vec{r})p^{\alpha}(\vec{r})\left\{-\frac{1}{2}[\phi(\vec{r})+v_n(\vec{r})]-v_{\rm xc}(\vec{r})+\varepsilon_{\rm xc}(\vec{r})\right\}d\vec{r}, \tag{34}$$

$$R_2^{\alpha}=\frac{1}{2}\sum_{A\in\alpha}Z_A\sum_{B\neq A}\left\{\frac{Z_B}{R_{AB}}-\int\frac{\rho_0^B(|\vec{r}-\vec{R}_B|)}{|\vec{r}-\vec{R}_A|}d\vec{r}\right\}+\frac{1}{2}\sum_{A\in\alpha}Z_A\int\frac{\rho_0^A(|\vec{r}-\vec{R}_A|)}{|\vec{r}-\vec{R}_A|}d\vec{r}-\frac{1}{2}\sum_{A\in\alpha}\int\frac{Z_A\tilde{\rho}_{\rm def}(\vec{r})}{|\vec{r}-\vec{R}_A|}d\vec{r}, \tag{35}$$

where the total density has been expressed as the sum of the spherical atomic density and the deformation density as defined in Eq. (21). In Eq. (35) the first two terms are short ranged while the last term with $\tilde{\rho}_{\rm def}(\vec{r})$ is long ranged. The long-range term can be computed in the same way as the deformation potential in Eq. (26).

The cohesive energy per atom is

$$E_c=\left(\sum_{A\in\alpha}E_0^A-E^{\alpha}\right)\Big/N^{\alpha}, \tag{36}$$

TABLE II. The cohesive energies (a.u.) per atom of lithium, copper, diamond, silicon, and sodium chloride for different k_A values from the modified local-projection method. The experimental lattice constants (3.491 Å for lithium, 3.567 Å for diamond, 5.430 Å for silicon, 5.610 Å for sodium chloride, and 3.60 Å for copper) and the fourth buffer scheme are used in all calculations. Three basis sets (S, D, and P) are used in the lithium calculations and the minimal basis sets (S) for others. See Sec. IV for details.

k_A	Li			Cu	Diamond	Si	NaCl
	S	D	P				
1	0.04275	0.05615	0.06353	0.09384	0.25262	0.16277	0.15297
5	0.04316	0.05653	0.06345	0.10024	0.30106	0.16560	0.15364
10	0.04324	0.05657	0.06342	0.10354	0.30239	0.16561	0.15381
15	0.04329	0.05663	0.06342	0.10600	0.30271	0.16560	0.15393
20	0.04331	0.05667	0.06342	0.10806	0.30290	0.16560	0.15403

where E^α is the total energy per primitive cell, E_0^A is the energy for isolated atom A (determined from our Kohn-Sham atomic program), and N^α is the number of atoms per primitive cell. In all the calculations, the inverse temperature β is set to 300 atomic units. For the exchange-correlation energy functional, the LDA in the Vosko-Wilk-Nusair (VWN) parametrization is used.[56]

IV. RESULTS AND DISCUSSION

Before we present the results for various solids from the divide-and-conquer calculations, we here demonstrate the accuracy and stability of the modified local-projection method described in Sec. III C. We show in Table II the cohesive energies per atom of lithium, copper, diamond, silicon, and sodium chloride for different k_A values (from Harris functional[57] calculations with the fourth buffer scheme as defined in Table I). The results indicate that except for some very small values, the total energies are generally insensitive to the change in k_A (energy difference normally around 10^{-4} to 10^{-3} hartree). We have chosen k_A to be 1.0, 5.0, 10.0, 10.0, and 10.0 for the calculations on lithium, copper, diamond, silicon, and sodium chloride, respectively. We now describe our calculations in detail.

A. Lithium

As the first example we have chosen metallic lithium. Lithium is a typical alkali metal and has been extensively studied by a large number of experimental techniques and theoretical methods.[58–63] It is well known that the valence electrons in bulk lithium behave almost like free electrons. Since the divide-and-conquer method is based on a localized description of the electronic structure, it is particularly interesting to see how the method performs for such a delocalized system.

We divide bcc bulk lithium into primitive cells with only one atom as a subsystem in each cell. The buffer schemes are presented in Table I. The cutoff radius for the short-range summation, R_{short}, is chosen as 30 a.u. The integration accuracy of 10^{-5} a.u. for density and electrostatic energy is used throughout all our calculations. In the lithium case this corresponds to about 3000 integration points per atom and generally leads to sufficient accuracy. The basis set plays an important role in the *ab initio* studies of metals. Three numerical atomic basis sets[36] are used here: the single (S) set for the minimal basis set ($2s$ functions), the double (D) set for double functions for valence atomic orbitals ($3s$ functions), and the polarization (P) set for the inclusion of polarization functions ($3s$ and $1p$ functions). The calculated ground-state properties of metallic lithium from the divide-and-conquer method are summarized in Table III.

To test the total-energy convergence with respect to buffer atoms, we have carried out a series of self-consistent divide-and-conquer calculations for bulk lithium with up to the fifth buffer scheme considered. The experimental lattice constant of 3.491 Å was used in the calculations. In Fig. 1 we plot the absolute values of errors in total energy per primitive cell as a function of the buffer atoms used. We observe that with the increasing use of buffer atoms the errors in total energy per primitive cell can be reduced to the values (10^{-3} hartree or less) which are within the inherent linear combination of atomic orbitals (LCAO) basis set errors. It is encouraging to notice that the convergence behavior of the total energy with respect to buffer atoms for this nearly-free-electron system is similar to that of a tetrapeptide molecule.[36] The calculated cohesive energies for S, D, and P sets are 1.14, 1.47, and 1.74 eV/atom, respectively, which compare well with the LDA band-structure results and the experimental value of 1.66 eV/atom.[63] All these seem to confirm that the divide-and-conquer approach, which only uses the local orbitals to represent the density, is capable of describing the electronic structure of systems with delocalized electrons.

TABLE III. Comparison of the ground-state properties for metallic lithium from the divide-and-conquer (DC) method, other theoretical calculations, and experiments. The P basis set and the fourth buffer scheme are used in all DC calculations.

Method	Cohesive energy (eV/atom)	Lattice constant (Å)	Bulk modulus (Mbar)
DC	1.74	3.42	0.116
KKR[a] (Ref. 58)	1.65	3.40	0.15
GTO[b] (Ref. 62)	1.65	3.45	0.138
Expt. (Ref. 61)	1.66	3.491	0.123

[a]Korringa-Kohn-Rostoker.

[b]Gaussian-type orbitals.

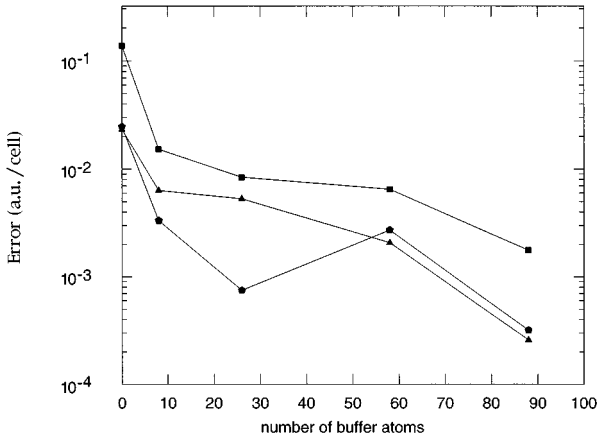

FIG. 1. Errors in the divide-and-conquer total self-consistent-field (SCF) energies per primitive cell as a function of the buffer atoms used for bulk lithium. The energies from the calculations that use the fifth buffer scheme are taken as references for S, D, and P basis sets. The square is for the S set, triangle for D set, and pentagon for P set.

To determine the equilibrium lattice constant and bulk modulus for lithium, we have performed a set of calculations using the P basis set to obtain the total self-consistent field (SCF) energies per primitive cell with the lattice constant varied from 3.09 to 3.79 Å. The cohesive energies and corresponding primitive cell volumes are then fitted to the widely used Murnaghan equation of state:[64]

$$E(V)=E(V_0)+\frac{B_0V}{B_0'(B_0'-1)}\left\{B_0'\left[1-\frac{V_0}{V}\right]+\left[\frac{V_0}{V}\right]^{B_0'}-1\right\}, \tag{37}$$

where V_0 is the equilibrium volume, B_0 the bulk modulus, and B_0' the pressure derivative of B_0. We display the results for the third and fourth buffer schemes with the P basis set in Fig. 2. Both fitting curves are closely parallel to each other, which means the good convergence of structural properties with respect to buffer atoms. The calculated cohesive energy, equilibrium lattice constant, and bulk modulus are 1.67 eV/atom, 3.41 Å, and 0.116 Mbar for the third buffer scheme and 1.74 eV/atom, 3.42 Å, and 0.116 Mbar for the fourth. These results are in good agreement with those from the LDA band-structure calculations and experimental values (see Table III).

To investigate the performance of the divide-and-conquer method on metallic lithium, we computed the total electronic density of states (DOS). Density of states is an important single-electron quantity which can give us insight into many phenomena related to solids. Most of the electronic properties of metals are determined by those electronic states near the Fermi energy. Since the divide-and-conquer approach does not involve a set of global single-electron eigenstates, the calculation of the DOS for metallic lithium provides a stringent test for the method. Presented in Figs. 3(a) and 3(b) are the calculated DOS curves near the Fermi energy for bulk lithium with the use of the P set and the fourth and fifth buffer schemes. Both curves clearly indicate that lithium is a metal. The Fermi energy in Fig. 3(a) agrees well with the one in Fig. 3(b). Although the major features such as the widths

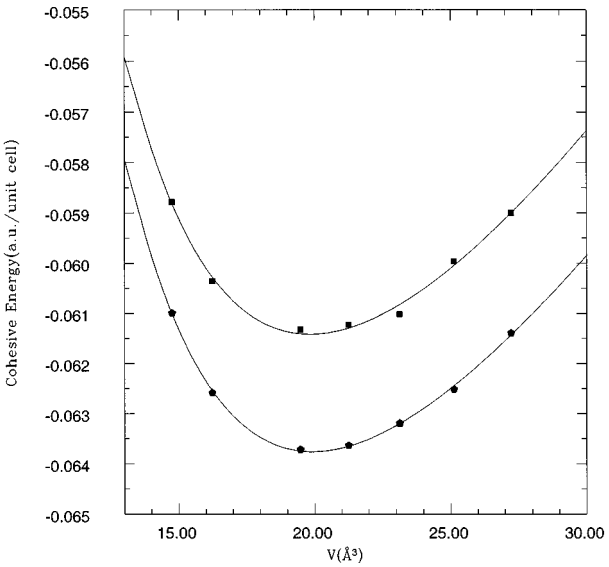

FIG. 2. Equation of state for bulk lithium. The P basis set is used in the calculations. The square is for the third buffer scheme and the pentagon for the fourth.

and locations of the corresponding peaks in Figs. 3(a) and 3(b) are quite similar, differences between the two curves do exist. It seems that the DOS quantity is more sensitive to the buffer scheme used than the cohesive energy and structural properties.

B. Copper

Copper is a transition metal and presents a challenging problem for the theoretical determination of its electronic structure.[65] It has a special electronic configuration with a filled outer $3d$ shell and a half-filled $4s$ valence orbital. The correct description of both the highly localized $3d$ states and

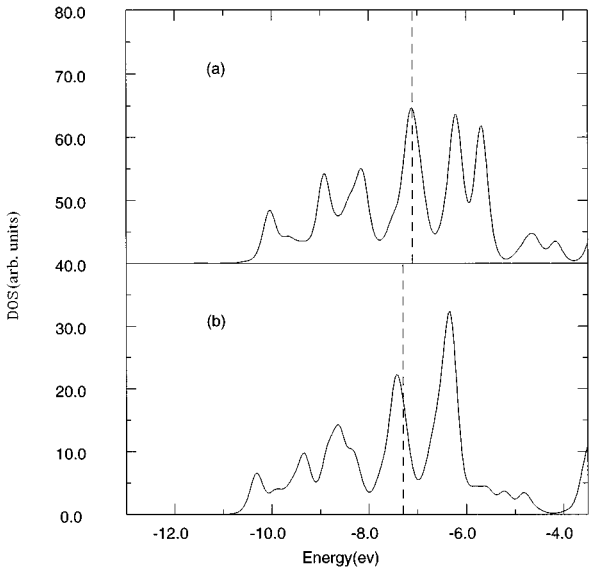

FIG. 3. The total density of states for bulk lithium. The calculations are performed with the P basis set. (a) is for the fourth buffer scheme and (b) for the fifth. The Fermi energy is indicated by the dashed line in each figure.

TABLE IV. Ground-state properties for fcc copper. Other LDA calculations and experimental values are listed for comparison.

Method	Cohesive energy (eV/atom)	Lattice constant (Å)	Bulk modulus (Mbar)
DC	4.49[a]	3.58[b]	1.67[b]
FLAPW[c] (Ref. 65)	4.14	3.60	1.62
KKR (Ref. 58)	4.08	3.58	1.55
LCAO (Ref. 10)	4.27	3.55	1.67
Expt. (Refs. 63, 65 and 66)	3.48	3.60	1.37,1.42

[a]Calculations with the *D* basis set and fourth buffer scheme.
[b]Calculations with the *S* basis set and fourth buffer scheme.
[c]Full-potential linearized augmented plane wave.

the loosely bound 4*s* state can be considered as a stringent test for any first-principles method. Therefore it is interesting to see how the divide-and-conquer method performs for this system.

The face-centered cubic (fcc) copper crystal is divided into primitive cells with only one atom (one subsystem) in each cell. The cutoff radius for the short-range summation is chosen as 35 a.u. About 6000 integration points per copper atom are needed to achieve the integration accuracy of 10^{-5} a.u. Two basis sets (*S* and *D*) are used in our calculations. The calculated ground-state properties of metallic copper from the divide-and-conquer method are summarized in Table IV. We have performed self-consistent divide-and-conquer calculations for bulk copper with up to the fifth buffer scheme considered. The absolute values of the errors in total energies per primitive cell are plotted as a function of the number of buffer atoms in Fig. 4. The experimental lattice constant of 3.60 Å was used in all calculations.[66] From Fig. 4 we notice that the errors in total energy per primitive cell decrease monotonically with the increasing use of buffer atoms (about 1.6 millihartree with 54 buffer atoms used). The cohesive energies determined from *S* and *D* set calculations are 2.75 and 4.49 eV/atom, respectively, against the experimental value of 3.49 eV/atom.[65] Previous calculations show that the LDA normally overestimates the cohesive energy of copper by about 20–40 % (see Table IV).[10]

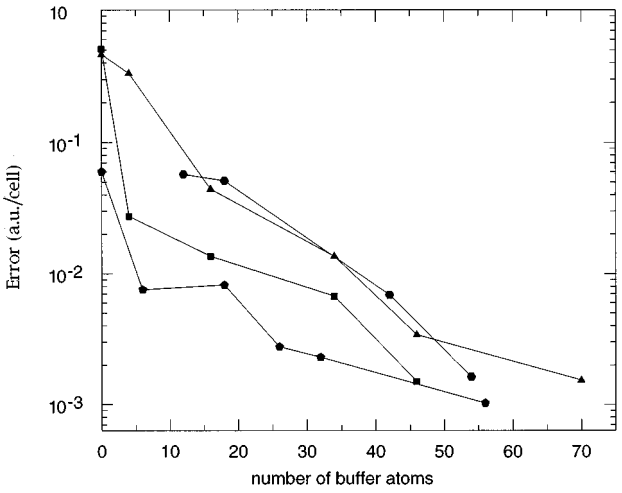

FIG. 4. Errors in the divide-and-conquer total SCF energies per primitive cell as functions of the buffer atoms used for diamond (triangle), silicon (square), sodium chloride (pentagon), and copper (hexagon). For diamond and sodium chloride, the energies from the calculations that use the sixth buffer scheme are taken as the references. For silicon and copper, the energies from the calculations that use the fifth buffer are taken as the references. The minimal basis set is used in all calculations.

We have fitted the Murnaghan equation of state for copper from the calculations which use the third and fourth buffer schemes with the *S* basis set. The calculated cohesive energy, equilibrium lattice constant, and bulk modulus are 3.79 eV/atom, 3.59 Å, and 1.77 Mbar for the third buffer scheme and 3.90 eV/atom, 3.58 Å, and 1.67 Mbar for the fourth. Overall our structural data are in good agreement with the experimental and other LDA results (see Table IV). The accuracy of these computed cohesive properties mainly depends on the accuracy of our total-energy calculations. For cohesive energy and lattice constant, we have found that the uncertainties associated with numerical integrations in these two sets of numbers are typically small (less than 1%). However, the bulk modulus data are strongly affected by the numerical accuracy in our total-energy calculations (the errors can be as large as 20%).

Presented in Figs. 5(a) and 5(b) are the calculated DOS curves near the Fermi energy for bulk copper with the use of the third and fourth buffer schemes. The sharp peaks below the Fermi energy (the nearest position to ε_F is about 2.08 eV) obviously have contributions from the highly localized filled *d* states. The relatively flat and extended peaks correspond to the loosely bound *s*-*p* states at about 9.77–10.54 eV, which is in good agreement with other LDA calculation results[65,67] (9.88–10.26 eV) and the experimental valence-band width of 8.6 eV.[68]

C. Diamond

Diamond serves as a typical covalently bonded insulator. The electronic structure of diamond crystal has been well established both theoretically and experimentally.[69–77] The localized electron density distribution and the highly directional sp^3 bonding in diamond certainly provide a significant

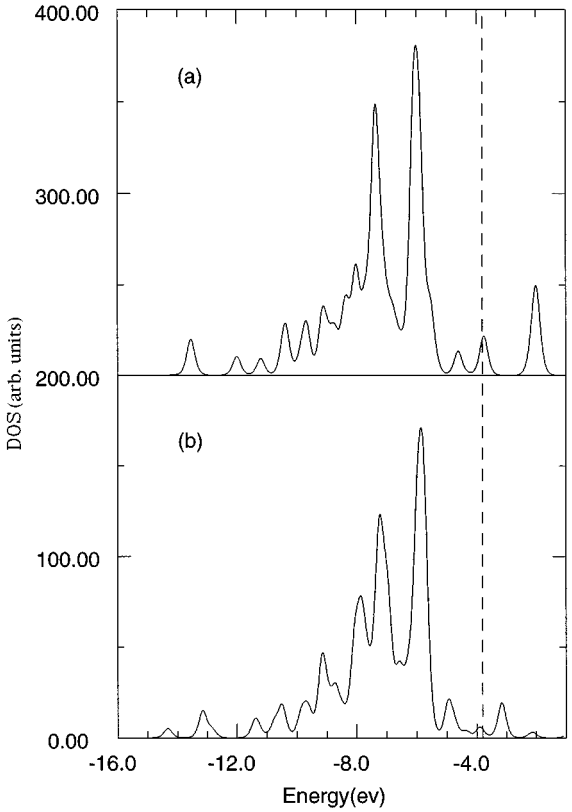

FIG. 5. The total density of states for fcc copper. The calculations are performed with the *S* basis set. (a) is for the third buffer scheme and (b) for the fourth. The Fermi energy is indicated by the dashed line in each figure.

test for any computational method in its ability to accurately represent the large deviations from the superimposed spherical densities and potentials.

The diamond crystal is partitioned into primitive cells with two atoms in one cell. Each primitive cell is further divided into two subsystems with only one carbon atom in each subsystem. For every subsystem, the surrounding buffer atoms and the corresponding buffer schemes are determined. The results are tabulated in Table I. We need about 4000 integration points to achieve the integration accuracy of 10^{-5} a.u. The short-range summation cutoff, R_{short}, is set to 35 a.u. Previous *ab initio* calculations on diamond seem to suggest that the minimal basis set is already good enough for many purposes[72–75] so we only use the *S* set $(2s/1p)$ throughout our calculations. The calculated cohesive energy and structural properties are listed in Table V. We show in Fig. 4 the convergence of the total energy per primitive cell with respect to the buffer atoms included in the calculations. We observe that the convergence is very smooth and roughly 70 buffer atoms are needed to bring the errors in total energy around 1 millihartree. Our computed cohesive energy is 8.11 eV/atom, against the experimental value of 7.37 eV/atom.[63] As many calculations have shown, the LDA normally overestimates cohesive energy.[10] The cohesive energy, equilibrium lattice constant, and bulk modulus from the fitted Murnaghan equation of state for diamond are 7.55 eV/atom, 3.56 Å, and 3.86 Mbar for the second buffer scheme and 7.96 eV/atom, 3.53 Å, and 4.19 Mbar for the third. The agreement between these two sets of data and other LDA results (see Table V) as well as with the experimental values is excellent. We have noticed that the structural properties for diamond converge more easily with respect to buffer schemes than those for lithium. This is probably due to the fact that diamond has a very large bulk modulus. Figures 6(a) and 6(b) show the DOS curves for the fifth and sixth buffer schemes. Although the details of the two curves do not match very well, both curves give almost the same energy gap of 6.0 eV for diamond, compared with the experimental gap of 5.4 eV.[63]

TABLE V. Ground-state properties for diamond. Other theoretical results and experimental values are listed for comparison. The minimal basis set is employed in all divide-and-conquer (DC) calculations.

Method	Cohesive energy (eV/atom)	Lattice constant (Å)	Bulk modulus (Mbar)
DC	8.11[a]	3.53[b]	4.19[b]
Plane wave (Ref. 73)	7.58	3.602	4.33
Local orbital (Ref. 74)	7.84	3.560	4.37
Hartree-Fock (Ref. 72)	5.69	3.59	5.9
Expt. (Ref. 74)	7.37	3.567	4.42

[a]Calculations with the sixth buffer scheme.
[b]Calculations with the third buffer scheme.

D. Silicon

We take the silicon crystal as the example of the application of the divide-and-conquer method to semiconductors. Silicon has the same crystal structure as diamond and has also been thoroughly investigated by numerous experimental and theoretical approaches, due to its technical importance in semiconductor technology.[10,63,78–82]

The partition scheme is the same as the one for diamond. We set $R_{\text{short}} = 50$ a.u. For simplicity we only used the

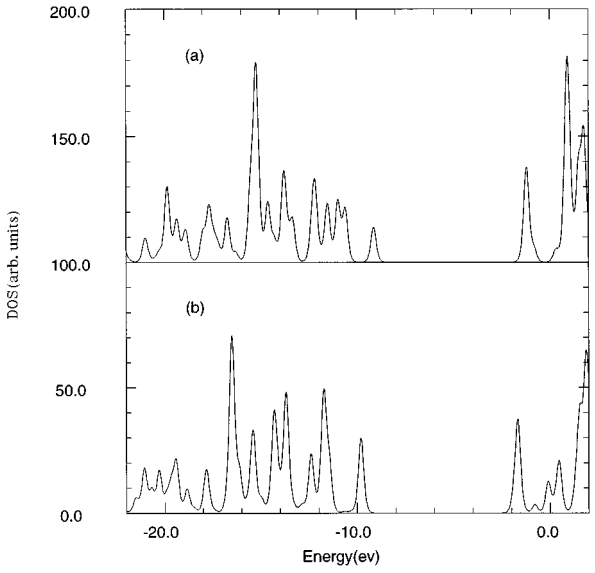

FIG. 6. The total density of states for diamond. The calculations are performed with the minimal basis set. (a) is for the fifth buffer scheme and (b) for the sixth.

TABLE VI. Ground-state properties for silicon. Other theoretical results and experimental values are listed for comparison. The minimal basis set is used in all divide-and-conquer (DC) calculations.

Method	Cohesive energy (eV/atom)	Lattice constant (Å)	Bulk modulus (Mbar)
DC	4.52[a]	5.42[b]	0.80 [b]
Plane wave (Ref. 80)	4.68	5.451	0.98
Plane wave (Ref. 81)		5.427	0.855
Plane wave (Ref. 82)		5.37	0.89
GTO (Ref. 78)	4.90	5.350	1.15
LMTO[c] (Ref. 79)	4.98	5.410	1.0
Local orbital (Ref. 10)	5.25	5.429	0.95
Expt. (Ref. 10)	4.63	5.43	0.99

[a]Calculations with the fifth buffer scheme.
[b]Calculations with the third buffer scheme.
[c]Linear muffin-tin orbitals.

minimal basis set $(3s/2p)$ in our calculations. The convergence curve of the total energy per primitive cell with respect to buffer atoms, shown in Fig. 4, is similar to that of diamond. Note that the total energy converges faster for silicon than for diamond in the sense that fewer buffer atoms are needed to reduce the error in total energy to a certain tolerance. This probably lies in the fact that with the same crystal structure silicon has a much larger lattice constant than diamond. The calculated cohesive energy, equilibrium lattice constant, and bulk modulus can be found in Table VI. They are overall in good agreement with other LDA and experimental results. The DOS curves of silicon presented in Figs. 7(a) and 7(b) for the fourth and fifth buffer schemes both give band gap of about 2.0 eV against the experimental value of 1.14 eV at 300 K.[63]

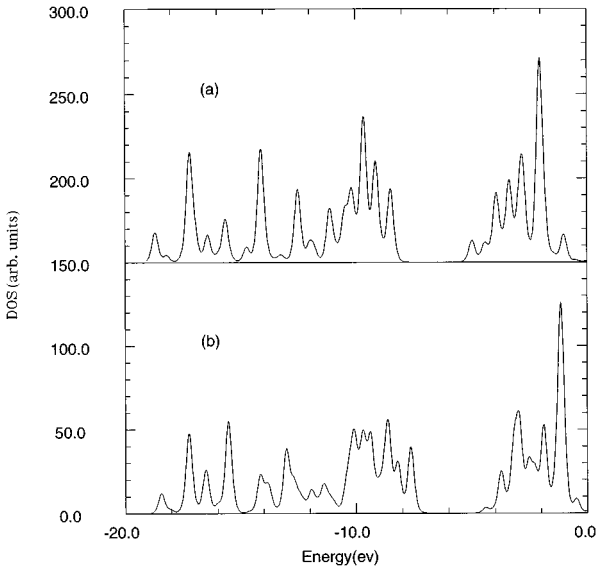

FIG. 7. The total density of states for silicon. The calculations are performed with the minimal basis set. (a) is for the fourth buffer scheme and (b) for the fifth.

TABLE VII. Ground-state properties for sodium chloride. Other LDA calculations and experimental values are listed for comparison.

Method	Cohesive energy (eV/atom)	Lattice constant (Å)	Bulk modulus (Mbar)
DC	4.21[a]	5.50[b]	0.308[b]
FLAPW (Ref. 83)	4.14	5.64	0.304
ASW [c] (Ref. 84)	4.05	5.40	0.32
LCAO (Ref. 10)	4.41	5.48	0.315
Expt. (Refs. 63, 83, and 85)	4.03	5.61	0.266

[a]Calculations with the *P* basis set and the fifth buffer scheme.
[b]Calculations with the *S* basis set and the third buffer scheme.
[c]Augmented spherical wave.

E. Sodium chloride

We finally apply the divide-and-conquer method to the calculation of an ionic crystal, sodium chloride. This typical ionic solid has been thoroughly investigated by numerous experimental[63,83,85,86] and theoretical approaches.[10,83,84,87,88] For ionic crystals like NaCl, the long-range interactions between ions should be taken into consideration very carefully in any accurate total-energy calculations. Many methods exist to deal with the divergence and conditional convergence problems related to the Madelung summation of the long-range potential. One of the well-known efficient summation schemes is the Ewald technique,[54] in which the lattice sum is divided into two, both rapidly convergent, summations, in real space and k space. In our potential scheme, the Coulomb potential is first obtained from the electron density calculated inside the short-range space ($R_{\text{short}}=$ 58 a.u. for NaCl) by solving the Poisson equation, and then outside this range to infinity the potential is computed with the conventional Ewald point charge model. Our calculated ground-state properties for NaCl from this potential scheme suggest that it works very well for ionic crystals.

The NaCl crystal is divided into primitive cells with two ions in one cell. Each primitive cell is further divided into two subsystems with only one Na or Cl ion in each subsystem. The buffer schemes for NaCl crystal are listed in Table I. About 4000 integration mesh points per atom are needed to achieve the numerical precision of 10^{-5}. Besides the *S* (single) basis set, the *D* (double) basis set and *P* (polarization including *d* functions for Na and Cl atoms) basis set are also used to obtain more accurate cohesive energy. The calculated ground-state properties are listed in Table VII.

The convergence of the total energy per unit cell with respect to the number of buffer atoms is shown in Fig. 4. The behavior of the convergence for NaCl is much better than those of lithium and diamond. In fact, the total energy is converged to 2×10^{-3} hartree for the fourth buffer scheme (with only 32 buffer atoms included) and 1×10^{-3} hartree for the fifth buffer scheme (56 buffer atoms). The good convergence in total energy for NaCl can be attributed to its well-localized electrons, which can be accurately and efficiently described by the divide-and-conquer strategy. The calculated cohesive energies with respect to the ions are

3.81, 4.17, and 4.21 eV/atom for *S*, *D*, and *P* basis sets, respectively, which are in good agreement with other LDA results (see Table VII). Again, the LDA slightly overestimate the cohesive energy compared with the experimental value.

The fit to the well-known Murnaghan equation of state is excellent for the fourth, fifth, and sixth buffer schemes. The cohesive energy, equilibrium lattice constant, and bulk modulus from the fitting curves are 3.85 eV/atom, 5.40 Å, and 0.318 Mbar for the fourth buffer scheme, 3.82 eV/atom, 5.45 Å, and 0.313 Mbar for the fifth, and 3.81 eV/atom, 5.50 Å, and 0.308 Mbar for the sixth. With increasing buffer atoms, our calculated structural parameters converge very well to the experimental results (see Table VII).

The total DOS curves calculated with the fourth, fifth, and sixth buffer schemes are plotted in Figs. 8(a)–8(c). Compared to the DOS for the fourth buffer scheme, the DOS from the fifth is closer to that of the sixth. The band gap obtained from the sixth buffer DOS curve is about 5.8 eV, against the experimental result of 8.6 eV.[86] It is well known that the LDA normally underestimates the experimental band gaps by 30–50 % for highly localized insulators.[87] Other LDA calculations give about 4.7 eV for the band gap.[88]

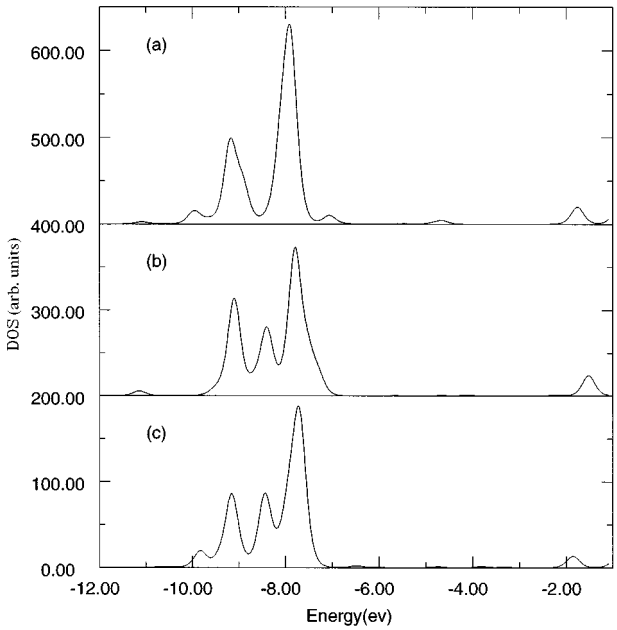

FIG. 8. The total density of states for sodium chloride. The calculations are performed with the minimal basis set. (a), (b), and (c) are for the fourth, fifth, and sixth buffer schemes, respectively.

V. SUMMARY

We have presented in this paper the divide-and-conquer density-functional approach for solid-state systems. The method directly determines the electronic structure of periodic solids without involving band structure. Our successful applications of this approach to four qualitatively different solid-state systems (metal, insulator, semiconductor, and ionic solid) have clearly demonstrated the utility of the method. In particular, we see from Fig. 4 that in our ''divide-and-conquer embedding'' scheme, one typically only needs about 40 to 50 buffer atoms to converge the cohesive energy to around 0.1 eV. But for all the solid-state systems considered in this paper, it appears that the DOS quantity is much more difficult to converge with respect to the size of the buffer cluster (see Fig. 5 to Fig. 8). The divide-and-conquer method can also be easily applied to extended solid-state systems without translational symmetry. The implementation of this method for theoretical investigations on adsorption and chemical reactions on surfaces is in progress.

ACKNOWLEDGMENTS

This research is supported by the National Science Foundation. We thank Dr. Zhongxiang Zhou, Dr. Darrin M. York, Dr. Qingsheng Zhao, and Tai-sung Lee for helpful discussions and the North Carolina Supercomputing Center for CPU time. W.Y. acknowledges partial finanacial support from the Alfred P. Sloan Foundation.

[1] *Theory of Inhomogeneous Electron Gas*, edited by S. Lundqvist and N. H. March (Plenum, New York, 1983).
[2] *Density Functional Theory of Molecules, Clusters, and Solids*, edited by D. E. Ellis (Kluwer Academic Publishers, Dordrecht, 1995).
[3] R. G. Parr and W. Yang, *Density-Functional Theory of Atoms and Molecules* (Oxford University Press, New York, 1989).
[4] R. M. Dreizler and E. K. U. Gross, *Density-Functional Theory* (Springer-Verlag, Berlin, 1990).
[5] J. C. Slater, Phys. Rev. **51**, 846 (1937).
[6] J. Korriga, Physica **13**, 392 (1947); W. Kohn and N. Rostoker, Phys. Rev. **94**, 1111 (1954).
[7] D. E. Ellis and G. S. Painter, Phys. Rev. B **2**, 2887 (1970).
[8] E. J. Baerends, D. E. Ellis, and P. Ros, Chem. Phys. **2**, 41 (1973).
[9] B. Delley, J. Chem. Phys. **92**, 508 (1990).
[10] G. te Velde and E. J. Baerends, Phys. Rev. B **44**, 7888 (1991).
[11] A. Zunger and A. J. Freeman, Phys. Rev. B **15**, 4716 (1977).
[12] J. R. Chelikowsky and S. G. Louie, Phys. Rev. B **29**, 3470 (1984).
[13] S. C. Erwin, M. R. Pederson, and W. E. Pickett, Phys. Rev. B **41**, 10 437 (1990).
[14] W. Y. Ching, J. Am. Ceram. Soc. **73**, 3135 (1990).
[15] O. K. Andersen and R. G. Woolley, Mol. Phys. **26**, 905 (1973).
[16] G. S. Painter and F. W. Averill, Phys. Rev. B **28**, 5536 (1983).
[17] A. D. Becke, J. Chem. Phys. **88**, 2547 (1988).
[18] P. M. Boerrigter, G. te Velde, and E. J. Baerends, Int. J. Quantum Chem. **33**, 87 (1988).
[19] E. Wimmer, H. Krakauer, M. Weinert, and A. J. Freeman, Phys. Rev. B **24**, 864 (1981).
[20] D. R. Hamann, M. Schlüter, and C. Chiang, Phys. Rev. Lett. **43**, 1494 (1980).
[21] R. Car and M. Parrinello, Phys. Rev. Lett. **55**, 2472 (1985).
[22] M. P. Teter, M. C. Payne, and D. C. Allan, Phys. Rev. B **40**, 12 255 (1989).

[23] A. R. Williams, P. J. Feibelman, and N. D. Lang, Phys. Rev. B **26**, 5433 (1982).
[24] P. J. Feibelman, Phys. Rev. Lett. **54**, 2627 (1985).
[25] M. C. Lega and S. C. Ying, Solid State Commun. **40**, 37 (1981).
[26] A. Zunger, Solid State Phys. **39**, 275 (1986).
[27] C. E. Dykstra and B. Kirtman, Annu. Rev. Phys. Chem. **41**, 155 (1990).
[28] T. B. Grimley, in *Electronic Structure and Reactivity of Metal Surfaces*, edited by E. G. Derouane and A. A. Lucas (Plenum, New York, 1976).
[29] D. E. Ellis, G. A. Benesh, and E. Byrom, Phys. Rev. B **16**, 3308 (1977).
[30] C. Pisani, Phys. Rev. B **17**, 3143 (1978); C. Pisani, R. Dovesi, and P. Carosso, *ibid.* **20**, 5345 (1979).
[31] J. L. Whitten and T. A. Pakkanen, Phys. Rev. B **21**, 4357 (1980); H. Yang and J. L. Whitten, Surf. Sci. **255**, 193 (1991).
[32] Y. Guo, J. M. Langlois, and W. A. Goddard III, Science **239**, 896 (1988).
[33] D. E. Ellis and J. Guo, in *Density Functional Theory of Molecules, Clusters, and Solids* (Ref. 2).
[34] W. Yang, Phys. Rev. Lett. **66**, 1438 (1991).
[35] C. Lee and W. Yang, J. Chem. Phys. **96**, 2408 (1992).
[36] W. Yang, Phys. Rev. A **44**, 7823 (1991).
[37] Z. Zhou, Int. J. Quantum Chem. Symp. **27**, 355 (1993).
[38] P. Cortona, Phys. Rev. B **44**, 8454 (1991).
[39] S. Baroni and P. Giannozzi, Europhys. Lett. **17**, 547 (1992).
[40] G. Galli and M. Parrinello, Phys. Rev. Lett. **69**, 3547 (1992).
[41] F. Mauri, G. Galli, and R. Car, Phys. Rev. B **47**, 9973 (1993).
[42] P. Ordejón, D. A. Drabold, M. P. Grumbach, and R. M. Martin, Phys. Rev. B **48**, 14 646 (1993).
[43] X. P. Li, R. W. Nunes, and D. Vanderbilt, Phys. Rev. B **47**, 10 891 (1993).
[44] M. S. Daw, Phys. Rev. B **47**, 10 895 (1993).
[45] D. A. Drabold and O. F. Sankey, Phys. Rev. Lett. **70**, 3631 (1993).
[46] W. Zhong, D. Tománek, and G. F. Bertsch, Solid State Commun. **86**, 607 (1993).
[47] A. Gibson, R. Haydock, and J. P. LaFemina, Phys. Rev. B **47**, 9229 (1993).
[48] M. Aoki, Phys. Rev. Lett. **71**, 3842 (1993).
[49] S. Goedecker and L. Colombo, Phys. Rev. Lett. **73**, 122 (1994).
[50] W. Kohn, Chem. Phys. Lett. **208**, 167 (1993).
[51] E. B. Stechel, A. P. Williams, and P. J. Feibelman, Phys. Rev. B **49**, 3898 (1993).
[52] W. Kohn and L. J. Sham, Phys. Rev. **140**, A1133 (1965).
[53] W. Yang and Z. Zhou, in *Density Functional Theory of Molecules, Clusters, and Solids* (Ref. 2).
[54] P. Ewald, Ann. Phys. (N.Y.) **64**, 253 (1921).
[55] W. Yang, J. Chem. Phys. **94**, 1208 (1991).
[56] S. H. Vosko, L. Wilk, and M. Nusair, Can. J. Phys. **58**, 1200 (1980).
[57] J. Harris, Phys. Rev. B **31**, 1770 (1985).
[58] V. L. Moruzzi, J. F. Janak, and A. R. Williams, *Calculated Electronic Properties of Metals* (Pergamon, New York, 1978).
[59] W. Y. Ching and J. Callaway, Phys. Rev. B **9**, 5115 (1974).
[60] J. L. Calais and G. Sperber, Int. J. Quantum Chem. **7**, 501 (1973).
[61] J. D. Pack, H. J. Monkhorst, and D. L. Freeman, Solid State Commun. **29**, 723 (1979).
[62] J. Callaway, X. Zou, and D. Bagayoko, Phys. Rev. B **27**, 631 (1983).
[63] C. Kittel, *Introduction to Solid State Physics* (Wiley, New York, 1976).
[64] F. D. Murnaghan, Proc. Natl. Acad. Sci. U.S.A. **3**, 244 (1944).
[65] M. H. Kang, R. C. Tater, E. J. Mele, and P. Soven, Phys. Rev. B **35**, 5457 (1987); J. R. Chelikowsky and M. Y. Chou, *ibid.* **38**, 7966 (1988).
[66] *American Institute of Physics Handbook*, 3rd ed. (McGraw-Hill, New York, 1972), Table 9d-3.
[67] Z. W. Lu, S.-H. Wei, and A. Zunger, Phys. Rev. B **41**, 2669 (1990).
[68] P. Thiry, D. Chanderis, J. Lecante, C. Guillot, R. Pinchanx, and Y. Petroff, Phys. Rev. Lett. **43**, 82 (1979).
[69] R. C. Chaney, C. C. Lin, and E. E. Lafon, Phys. Rev. B **3**, 459 (1971).
[70] G. S. Painter, D. E. Ellis, and A. R. Lubinsky, Phys. Rev. B **4**, 3610 (1971).
[71] A. Zunger and A. J. Freeman, Phys. Rev. B **15**, 5049 (1977).
[72] R. Dovesi, C. Pisani, F. Ricca, and C. Roetti, Phys. Rev. B **22**, 5936 (1980).
[73] M. T. Yin and M. L. Cohen, Phys. Rev. B **24**, 6121 (1981).
[74] J. R. Chelikowsky and S. G. Louie, Phys. Rev. B **29**, 3470 (1983).
[75] W. E. Pickett and C. S. Wang, Phys. Rev. B **30**, 4719 (1984).
[76] W. R. L. Lambrecht and O. K. Andersen, Phys. Rev. B **34**, 2439 (1986).
[77] *The Properties of Diamond*, edited by J. E. Field (Academic, London, 1979).
[78] J. R. Chelikowsky, S. G. Louie, D. Vanderbilt, and C. T. Chain, Int. J. Quantum Chem. Symp. **18**, 105 (1984).
[79] A. Svane, Phys. Rev. B **35**, 5496 (1987).
[80] M. T. Yin and M. L. Cohen, Phys. Rev. B **26**, 5668 (1982).
[81] P. E. Van Camp, V. E. Van Doren, and J. T. Devreese, Phys. Scr. **35**, 706 (1987).
[82] A. Oshiyama and M. Saito, J. Phys. Soc. Jpn. **56**, 2104 (1987).
[83] H. J. F. Jansen and A. J. Freeman, Phys. Rev. B **33**, 8629 (1986).
[84] C. S. Wang and J. Callaway, Comput. Phys. Commun. **14**, 327 (1978).
[85] H. Spetzler, C. G. Sammis, and R. J. O'Connell, J. Phys. Chem. Solids **33**, 1727 (1972); L. C. Chhabildas and A. L. Ruoff, J. Appl. Phys. **47**, 4182 (1976).
[86] S. Nakai and T. Sagawa, J. Phys. Soc. Jpn. **26**, 1427 (1969).
[87] R. A. Heaton and C. C. Lin, J. Phys. C **17**, 1853 (1984).
[88] K. A. Jackson and C. C. Lin, Phys. Rev. B **38**, 12 171 (1988).